

Anion Reorientations in the Superionic Conducting Phase of $\text{Na}_2\text{B}_{12}\text{H}_{12}$

Nina Verdal,^{†,‡} Terrence J. Udovic,^{*,†} Vitalie Stavila,[§] Wan Si Tang,^{†,‡} John J. Rush,^{†,‡}
and Alexander V. Skripov^{||}

[†]NIST Center for Neutron Research, National Institute of Standards and Technology, Gaithersburg, Maryland 20899-6102, United States

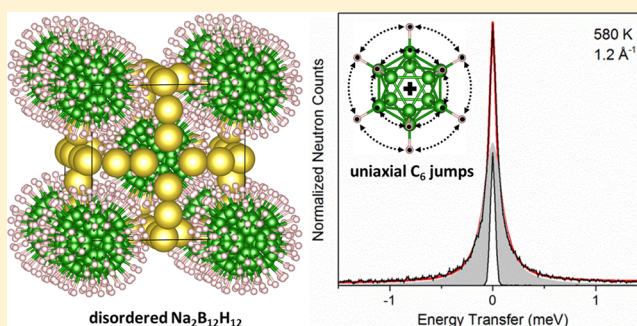
[‡]Department of Materials Science and Engineering, University of Maryland, College Park, Maryland 20742-2115, United States

[§]Sandia National Laboratories, Livermore, California 94551, United States

^{||}Institute of Metal Physics, Ural Branch of the Russian Academy of Sciences, Ekaterinburg 620990, Russia

S Supporting Information

ABSTRACT: Quasielastic neutron scattering (QENS) methods were used to characterize the reorientational dynamics of the dodecahydro-*closo*-dodecaborate ($\text{B}_{12}\text{H}_{12}^{2-}$) anions in the high-temperature, superionic conducting phase of $\text{Na}_2\text{B}_{12}\text{H}_{12}$. The icosahedral anions in this disordered cubic phase were found to undergo rapid reorientational motions, on the order of 10^{11} jumps s^{-1} above 530 K, consistent with previous NMR measurements and neutron elastic-scattering fixed-window scans. QENS measurements as a function of the neutron momentum transfer suggest a reorientational mechanism dominated by small-angle jumps around a single axis. The results show a relatively low activation energy for reorientation of 259 meV (25 kJ mol^{-1}).



INTRODUCTION

The dodecahydro-*closo*-dodecaborate ($\text{B}_{12}\text{H}_{12}^{2-}$) anions have received recent attention in hydrogen-storage research as they are potential byproducts formed by heating diborane with metal hydrides or by thermal decomposition of metal tetrahydroborates, $\text{M}(\text{BH}_4)_x$ (where M = alkali or alkaline-earth elements, $x = 1, 2$).^{1–13} The icosahedral $\text{B}_{12}\text{H}_{12}^{2-}$ anion is more stable than other borohydride anions because the $\text{B}_{12}\text{H}_{12}^{2-}$ boron cage is pseudoaromatic.^{14,15} Once formed during borohydride dehydrogenation, its stability stymies the rehydrogenation back to the parent borohydrides. Facile rehydrogenation is necessary for the proposed use of borohydrides as practical materials for mobile hydrogen storage.

On the other hand, the high thermal stability of the $\text{B}_{12}\text{H}_{12}^{2-}$ anion and its relatively large size and quasi-spherical shape (which tend to promote wider intralattice pathways for cation diffusion) are desirable qualities for its uses in solid-state, fast-ion conductor materials. This is reflected by the recent discovery of Na^+ superionic conduction in $\text{Na}_2\text{B}_{12}\text{H}_{12}$.¹⁶ At room temperature, the $\text{Na}_2\text{B}_{12}\text{H}_{12}$ structure is monoclinic with $P2_1/n$ symmetry.¹⁷ This ordered structure undergoes a hysteretic phase transition near 529 K upon heating, first to a partially disordered, pseudo-body-centered-cubic (bcc) structure with $Pm\bar{3}n$ symmetry, then to a slightly higher-temperature, fully disordered, bcc structure with $Im\bar{3}m$ symmetry¹⁸ (see Figure 1). These high-temperature structures exhibit anion

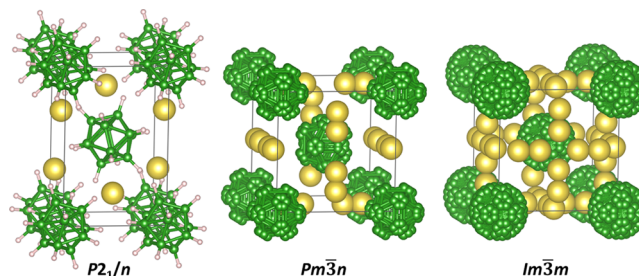


Figure 1. Depictions of the ordered monoclinic and disordered cubic structures for $\text{Na}_2\text{B}_{12}\text{H}_{12}$ from ref 18. Na, B, and H positions are depicted by gold, green, and pink atoms, respectively. Na site pairs in the disordered structures represent the possible off-center positioning within each corresponding tetrahedral interstice. H atoms are omitted from the disordered structures for clarity.

orientational disorder and are rich with cation vacancies. Upon transition to the high-temperature phases, there is about a 3-orders-of-magnitude increase in Na^+ cation conduction to near 0.1 S cm^{-1} , indicative of the onset of superionicity.¹⁶ Upon cooling, the disordered cubic structure reverts back to the ordered monoclinic structure below $\approx 480 \text{ K}$.

Received: June 24, 2014

Revised: July 17, 2014

Published: July 18, 2014

In addition to confirming an enhanced Na⁺ cation mobility of at least 2×10^8 jumps s⁻¹, previous NMR results¹⁹ indicated that the transformation from the low-temperature to high-temperature structures is also accompanied by about a 2-orders-of-magnitude increase in the anion reorientational jump rate to ca. 10^{11} jumps s⁻¹ and a nearly 3-fold decrease in the activation energy for reorientation. This behavior was corroborated by prior elastic neutron elastic scattering fixed-window scans,¹⁸ which also indicated a dramatic increase in anion reorientational jump rate upon transformation to the disordered cubic phases. The extent that anion reorientational mobility affects cation translational mobility is yet to be determined. Thus, it is desirable to gain more insight concerning the mechanistic details of the anion reorientations in superionic Na₂B₁₂H₁₂. In the current study, we have characterized the reorientational dynamics of the B₁₂H₁₂²⁻ anions in this high-temperature region by quasielastic neutron scattering (QENS).

EXPERIMENTAL METHODS

¹¹Boron-enriched Na₂¹¹B₁₂H₁₂ (and Na₂¹¹B₁₂D₁₂) was synthesized via ion exchange¹⁷ of Cs₂¹¹B₁₂H₁₂ (and Cs₂¹¹B₁₂D₁₂) acquired from Katchem²⁰ to generate aqueous [H₃O]₂¹¹B₁₂H₁₂ (and [H₃O]₂¹¹B₁₂D₁₂), followed by reaction with Na₂CO₃. (N.B., 20% of natural boron is ¹⁰B, which is a strong neutron absorber.) The resulting hydrated polycrystalline material was dried by dynamic vacuum at 523 K for 16 h. The sample material was handled in a He-filled glovebox and arranged annularly in an aluminum sample can for QENS measurements. The deuterated sample had a D:H ratio of 87:13 as determined from refinement of neutron powder diffraction data.¹⁸ Although only ¹¹B-enriched samples were used, we drop the explicit isotope designation throughout this paper for simplicity.

The QENS measurements were performed at the National Institute of Standards and Technology (NIST) Center for Neutron Research (NCNR) on the Disc Chopper Spectrometer²¹ (DCS) utilizing incident neutrons at 4.8 Å (3.55 meV) with a 56.1 μeV full width at half-maximum (FWHM) resolution. Spectra were collected over a momentum transfer (*Q*) range of 0.1 Å⁻¹ to 2.4 Å⁻¹. The instrument resolution function, *R(Q, ω)*, was determined from the measured QENS spectra for Na₂B₁₂H₁₂ (and Na₂B₁₂D₁₂) at low temperature (100 K), where the reorientational motion is “frozen” at the frequency scale of the spectrometer. The reduced data were analyzed using the DAVE software package.²² N.B., all vertical error bars in the accompanying figures of this paper denote ±1 σ.

RESULTS AND DISCUSSION

Quasielastic neutron scattering probes the reorientations of the B₁₂H₁₂²⁻ anions by the scattering of neutrons from primarily the hydrogen atoms. The observed QENS spectra (obs) are generally fit to a delta function, δ(ω), and a summation of Lorentzian functions, *L_i(ω)*, where

$$L_i(\omega) = \frac{1}{\pi} \frac{\frac{\hbar}{\tau_i}}{\left(\frac{\hbar}{\tau_i}\right)^2 + (\hbar\omega)^2} \quad (1)$$

(in which \hbar is the reduced Planck's constant, $\hbar\omega$ is the neutron energy transfer, τ_i are correlation times, and \hbar/τ_i are the Lorentzian half widths at half-maximum (HWHMs)), to represent the elastic and quasielastic scattering, respectively,

and convolved with the instrument resolution function, *R(Q, ω)*:

$$\text{obs} = S(Q, \omega) \otimes R(Q, \omega) = [A_0(Q)\delta(\omega) + \sum_i A_i(Q)L_i(\omega)] \otimes R(Q, \omega) \quad (2)$$

The term $[A_0(Q)\delta(\omega) + \sum_i A_i(Q)L_i(\omega)]$ represents the scattering function, *S(Q, ω)*, in which *A₀(Q)* is the elastic incoherent structure factor (EISF) and the *A_i(Q)* represent the quasielastic incoherent structure factors. An example of an observed spectrum and the functional fit is shown in Figure 2.

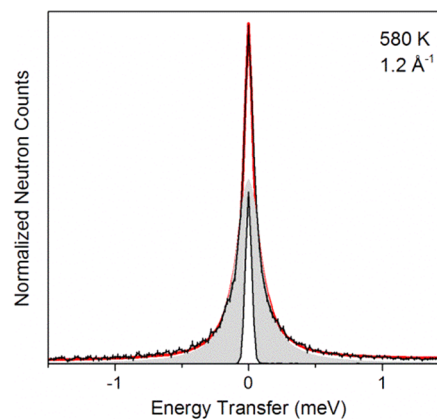


Figure 2. A quasielastic neutron scattering spectrum of Na₂B₁₂H₁₂ at 580 K at a momentum transfer of 1.2 Å⁻¹, using 4.8 Å incident neutrons. The red line is the fit to the data (black), with the functional components in white (elastic), and gray (quasielastic).

Since the QENS spectra are collected as a function of momentum transfer, the geometry of the reorientation can be deduced. The EISF is determined experimentally as the ratio of the elastic (incoherent) scattering intensity to the total (incoherent) scattering intensity, plotted as a function of momentum transfer. The total incoherent scattering intensity is the sum of the intensities of the elastic and quasielastic scattering, and follows the assumption that the quasielastic and vibrational motions are separable, occurring on different time scales. At higher temperatures, this assumption is no longer entirely valid, since there can be increasing overlap between inelastic and quasielastic scattering.

Because the reorientational jump rates are of the order of 10^9 jumps s⁻¹ or less in the low-temperature ordered structure,¹⁹ we focused our attention on the orders-of-magnitude more mobile B₁₂H₁₂²⁻ anions of the high-temperature disordered structures. The experimental EISFs were determined for Na₂B₁₂H₁₂, and the results were compared with geometrically feasible models for reorientation within the high-temperature bcc lattice. The EISF values were determined by fitting the quasielastic scattering to one Lorentzian at each *Q* value, even though as seen later, the actual quasielastic scattering may be the summation of multiple Lorentzian components of different widths and intensities. Typically, the one-Lorentzian simplification is sufficient to capture the relative total amount of quasielastic scattering intensity present compared to the elastic scattering intensity. The EISF curves for various reorientation models are compared in Figure 3 with the experimental data obtained at several temperatures, namely, at 580 and 620 K in the fully disordered *Im* $\bar{3}m$ structure and, after cooling, to 480 K

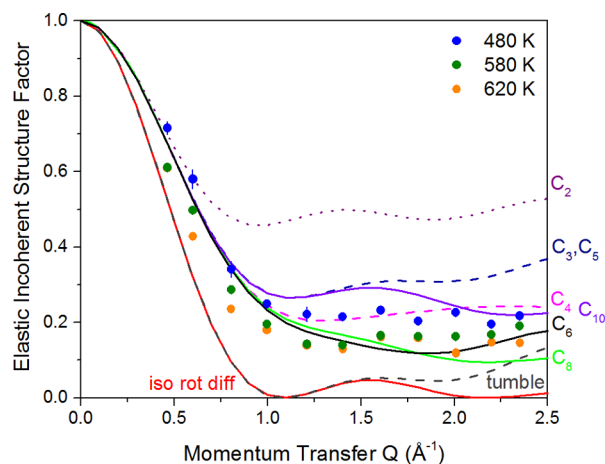


Figure 3. Experimental EISF values at 480 K (blue circles) for the partially disordered $Pm\bar{3}n$ structure, and at 580 K (green circles) and 620 K (orange circles) for the fully disordered $Im\bar{3}m$ structure compared with various uniaxial jump reorientation models: 2-fold (purple dots), 4-fold (pink dashes), and 8-fold (green line) jumps about the C_2 axis; 3-fold (blue dashes) and 6-fold (black line) jumps about the C_3 axis; and 5-fold (same as 3-fold, blue dashes) and 10-fold (purple line) jumps about the C_5 axis. Also shown are 3-D reorientation models: localized, discrete molecular tumbling (gray dashes) and isotropic rotational diffusion (red line).

in the partially disordered $Pm\bar{3}n$ structure. The somewhat higher EISF data points at 480 K compared to those at higher temperatures are consistent with the temperature behavior previously observed for the elastic-peak intensity of $Na_2B_{12}H_{12}$ during neutron elastic-scattering fixed-window scans.¹⁸

The models under consideration were those describing uniaxial jump reorientations around various icosahedral symmetry axes (see Figure 4), as well as three-dimensional (3-D) reorientations involving multiple axes. The presence of considerable anion orientational disorder in the high-temperature structures means that we had to also consider reorientation models that did not necessarily preserve a particular anion orientation at each lattice position. In other words, besides 2-fold (π) jumps around the C_2 symmetry axis,²³ 3-fold ($2\pi/3$) jumps around the C_3 symmetry axis,²³ and 5-fold ($2\pi/5$) jumps around the C_5 symmetry axis²³ of the icosahedral $B_{12}H_{12}^{2-}$ anion (all reorientations that rotate the icosahedral anion into an identical image of itself), we included the possibility of smaller jumps occurring around these same axes (see Figure 4). Figure 3 shows the effect on the EISF of

decreasing the jump distances around each of the three symmetry axes mentioned, i.e., 4-fold ($\pi/2$) and 8-fold ($\pi/4$) jumps around the C_2 symmetry axis, 6-fold ($\pi/3$) jumps around the C_3 symmetry axes, and 10-fold ($\pi/5$) jumps around the C_5 symmetry axes. Also shown for comparison are the EISF curves corresponding to 3-D tumbling among the 12 icosahedral H sites and the limiting case of isotropic rotational diffusion. All models are mathematically defined for comparison in the Supporting Information (SI).

On the time scale covered by DCS, the QENS data indicate that the anion reorientational mechanism is predominantly uniaxial in nature at all temperatures measured, since any 3-D mechanism (i.e., discrete tumbling or rotational diffusion) predicts a significantly lower EISF curve. Moreover, none of the fundamental uniaxial jump mechanisms that preserve a particular crystallographic anion orientation (i.e., π jumps around the C_2 axis, $2\pi/3$ jumps around the C_3 axis, or $2\pi/5$ jumps the C_5 axis) agrees with the observed EISF values, since they display much higher EISF curves. This is in contrast to what has been observed previously for the ordered $Fm\bar{3}$ phase of $Cs_2B_{12}H_{12}$, where the EISF values at 430 K clearly indicated orientation-preserving uniaxial jumps around the C_3 and/or C_5 axes.²³

It is clear from Figure 3 that good agreement requires a uniaxial reorientation model with much smaller jump distances to mimic the considerable orientational disorder experienced by each anion. Of the three symmetry axes considered, we can exclude reorientations around the C_5 symmetry axis no matter what the jump distances are, since the resulting EISF curves are always in poor agreement with the observed values. This particular axis precludes two axial H atoms from reorienting, so they scatter elastically, and has only one H radius of rotation, leading to the unusual shape of the EISF(Q) curve. In contrast, both C_2 and C_3 symmetry axes respectively possess three and two different H radii of rotation and all 12 H atoms participate in the reorientations. The observed EISF values appear to agree fairly well with models incorporating smaller jump reorientations around these axes. For the fully disordered $Im\bar{3}m$ structure at 580 and 620 K, the best overall agreement is seen for 6-fold ($\pi/3$) jumps around the C_3 axis, whereas for the partially disordered $Pm\bar{3}n$ structure at 480 K, the best overall agreement is seen for 4-fold ($\pi/2$) jumps around the C_2 axis. Thus, we focus our attention on a more detailed analysis of these two mechanisms.

Comparison of 6-Fold and 4-Fold Jump Models. The EISF expected for 6-fold reorientation of the $B_{12}H_{12}^{2-}$ anion

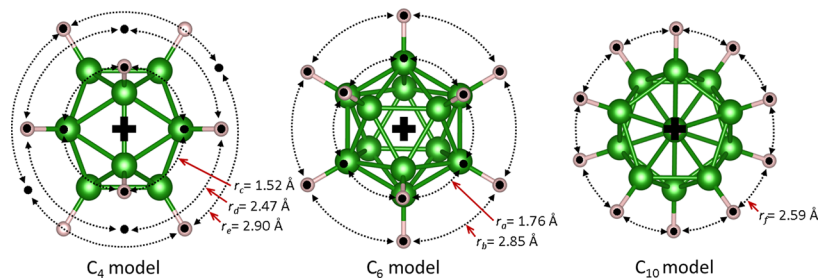


Figure 4. A schematic of $B_{12}H_{12}^{2-}$ uniaxial small-jump 4-fold (C_4 model), 6-fold (C_6 model), and 10-fold (C_{10} model) reorientations around the C_2 , C_3 , and C_5 local symmetry axes, respectively, with each axis (designated by the + symbol) oriented perpendicular to the page. Black circles represent the various equiangular positions of the reorienting H atoms. Respective larger-angle jump models described by 2-fold (C_2 model), 3-fold (C_3 model), and 5-fold (C_5 model) reorientations can be envisioned by doubling the allowable near-neighbor jump distances. The different reorientation radii are labeled accordingly.

about a single icosahedral C_3 axis (C_6 model) involves all 12 covalently bound H atoms jumping through the same angle simultaneously, but on circles of two different radii (see Figure 4). This EISF can be written as

$$A_0(Q) = \frac{1}{12} [2 + 2j_0(Qr_a) + 2j_0(Qr_a\sqrt{3}) + j_0(2Qr_a) + 2j_0(Qr_b) + 2j_0(Qr_b\sqrt{3}) + j_0(2Qr_b)] \quad (3)$$

in which r_a and r_b are the radii of the circles traced by the H atoms during the rigid-body reorientational motion and $j_0(x)$ is the zeroth order Bessel function of the first kind, equal to $\sin(x)/x$. Despite the different radii, each hydrogen atom possesses the same residence time between jumps and, therefore, contributes equally to the quasielastic line widths. Theoretically, three quasielastic features with HWHMs (\hbar/τ_i , $i = 1, 2, 3$) contribute to the spectra under the influence of this reorientation mechanism,²⁴ with $\tau_1 = 3\tau_2 = 4\tau_3 = 2\tau$, where τ is the mean residence time, equivalent to the inverse of the jump frequency. The relative intensities of the three Lorentzian functions as a function of Q are determined by the quasielastic incoherent structure factors, i.e., the $A_i(Q)$ functions found in eq 2 and defined in the SI.

These functions are plotted in Figure 5a with r_a and r_b values of 1.76 and 2.85 Å, respectively. Experimentally, the statistics of the data limit the ability to distinguish quasielastic features with similar line widths, especially if one quasielastic feature dominates the spectrum at a given Q . This is the reason that the EISF values were determined using one Lorentzian function at each temperature, for each Q value. The relative intensities of

the delta function (elastic scattering) and the Lorentzian function (quasielastic scattering) at 580 and 620 K are also plotted in Figure 5a, with the corresponding theoretical values for the C_6 model.

The EISF expected for 4-fold reorientation about a single icosahedral C_2 axis (C_4 model) involves all 12 H atoms jumping on circles of three different radii: r_c , r_d , and r_e (see Figure 4). This EISF can be written as

$$A_0(Q) = \frac{1}{12} [3 + 2j_0(Qr_c\sqrt{2}) + j_0(2Qr_c) + 2j_0(2Qr_d\sqrt{2}) + j_0(2Qr_d) + 2j_0(Qr_e\sqrt{2}) + j_0(2Qr_e)] \quad (4)$$

There are two quasielastic scattering Lorentzian features with $\tau_1 = 2\tau_2 = \tau$. The corresponding $A_i(Q)$ functions²⁴ are defined in the SI and are plotted in Figure 5b with r_c , r_d , and r_e values of 1.52 Å, 2.47 Å, and 2.90 Å, respectively. The relative intensities of the delta function (elastic scattering) and the Lorentzian function (quasielastic scattering) at 480 K are also plotted in Figure 5b, with the corresponding theoretical values for the C_4 model.

Activation Energy for Reorientation. In order to estimate a reorientational activation energy E_a over the entire temperature range, it is potentially more useful to compare the τ_1 correlation times rather than mean residence times τ . Dianoux et al.²⁵ have shown that for uniaxial small-jump reorientation models, the rotational diffusion constant D_r , in the limit of $Qr < \pi$, is approximately related to τ_1 by

$$D_r \simeq \frac{1}{\tau_1} = \frac{2}{\tau} \sin^2\left(\frac{\pi}{N}\right) \quad (5)$$

where N is the number of equiangular jump sites on a circle. It is clear that the relationship between τ_1 and τ depends on the value of N , which is directly related to the angular jump distance associated with a specific reorientation model. By considering τ_1 instead of τ , one can compare the temperature behavior of the first Lorentzian component (which also dominates at low Qr values), regardless of the particular small-jump uniaxial mechanism, and extract a meaningful estimate for the activation energy associated with the rotational diffusion constant. Another option is to use the same reorientation model (e.g., the C_6 model) at all temperatures at the lower Q values (where all models exhibit similar behavior) to extract τ values, and use these τ values to extract a reorientational activation energy. The obvious problem with comparing τ values calculated from two different models is that the meaning of τ is model-dependent, as shown in eq 5. Indeed, if the first Lorentzian component were analyzed with a C_4 model instead of a C_6 model, the resulting τ would be twice as large even though the τ_1 values are identical.

In the present case, we decided on the second option and determined τ values at all temperatures using the same C_6 jump model at lower Q values (eq 3 and eqs S1, S2, and S3 in the SI), with $\tau_1 = 2\tau$, even at 480 K, where the C_4 jump model somewhat better described the overall data. From this C_6 jump model, the resulting τ values were then fit as a function of temperature to an Arrhenius equation (Figure 6), yielding an activation energy of $259 \text{ meV} \pm 22 \text{ meV}$ ($25 \text{ kJ mol}^{-1} \pm 2 \text{ kJ mol}^{-1}$) from the $-E_a/k$ slope, where k is Boltzmann's constant.

This activation energy is in agreement with the value of 270 meV determined for the high-temperature $\text{Na}_2\text{B}_{12}\text{H}_{12}$ phase from measurements of ^1H and ^{11}B NMR spin–lattice relaxation rates, and much lower than the 770 meV activation energy for

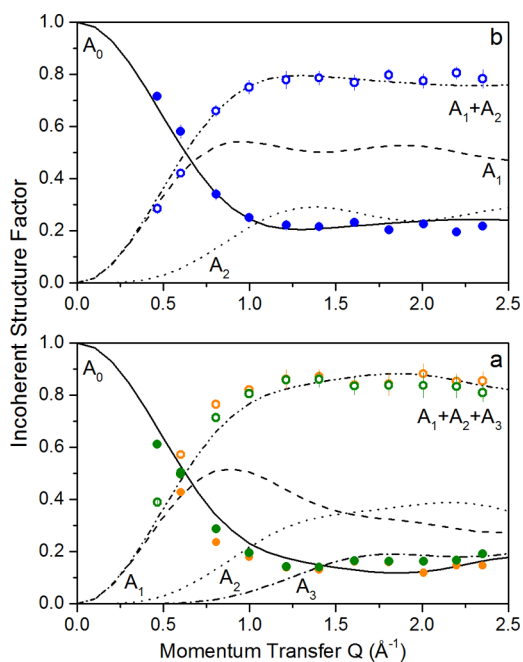


Figure 5. Incoherent structure factors plotted as a function of Q for (a) 6-fold ($\pi/3$) jumps about the C_3 axis (C_6 model) and (b) 4-fold ($\pi/2$) jumps about the C_2 axis (C_4 model) of the $\text{B}_{12}\text{H}_{12}^{2-}$ anion. The fitted elastic (solid circles) and quasielastic (empty circles) intensities as a function of Q for (a) 620 K (orange) and 580 K (green) compared to the calculated curves for the C_6 model, and (b) 480 K (blue) compared to the calculated curves for the C_4 model. The black lines denote the corresponding theoretical elastic and quasielastic intensities.

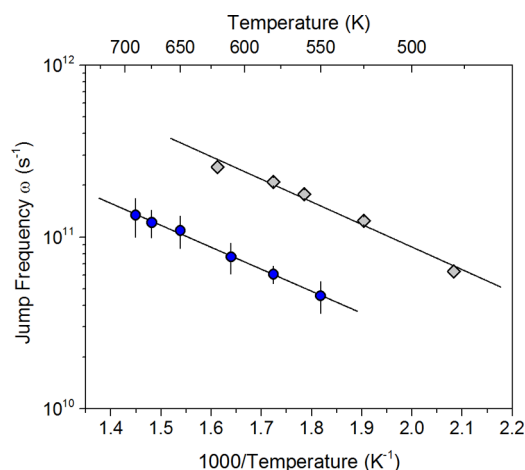


Figure 6. An Arrhenius plot for $\text{Na}_2\text{B}_{12}\text{H}_{12}$ (gray diamonds) and $\text{Na}_2\text{B}_{12}\text{D}_{12}$ (blue circles) from which the activation energies for the reorientational motion were determined. Jump frequencies are based on the $1/\tau$ values from the C_6 model.

anion reorientations in the low-temperature ordered monoclinic phase.¹⁹ Only as a result of the entropically driven phase transition at high temperatures do the anions lose so much resistance to reorientation. Similar to the anion reorientation barriers in $\text{Cs}_2\text{B}_{12}\text{H}_{12}$,²³ the activation energy for disordered $\text{Na}_2\text{B}_{12}\text{H}_{12}$, although only about one-third as large as that of the low-temperature ordered phase, is still equivalent to temperatures in excess of 3000 K and more than 20-fold larger than the anion torsional energies. Thus, it is clear that the anions in the high-temperature disordered phase are making small discrete reorientational jumps from deep within their torsional potential wells rather than undergoing quasi-free rotational diffusion.

Separate QENS experiments for $\text{Na}_2\text{B}_{12}\text{D}_{12}$ (albeit with 13% H) were performed in order to get an estimate of the jump frequencies and activation energy for $\text{B}_{12}\text{D}_{12}^{2-}$ reorientations. Even though the presence of both D and H with their vastly different coherent and incoherent neutron scattering cross sections complicates any detailed mechanistic analysis, we nonetheless assumed that the reorientation mechanism was isotope-independent and calculated τ values in a similar fashion by fitting the quasielastic component to three Lorentzians with relative intensities in accordance with the C_6 jump model. This resulted in an activation energy for the $\text{B}_{12}\text{D}_{12}^{2-}$ reorientations of $252 \text{ meV} \pm 7 \text{ meV}$ ($24.5 \text{ kJ mol}^{-1} \pm 0.7 \text{ kJ mol}^{-1}$), nearly the same as that for the hydrogenated sample, within the uncertainty of the calculation. At any given temperature, the approximate 3-fold decrease in jump rate for $\text{B}_{12}\text{D}_{12}^{2-}$ anions compared to that for $\text{B}_{12}\text{H}_{12}^{2-}$ anions probably reflects the slightly (1%)¹⁸ smaller lattice constant of the deuterated compound (steric effect), as well as the somewhat larger moment of inertia for the deuterated anion.

Consideration of Combined Models. As seen earlier, the QENS data at the higher temperatures are most consistent with reorientation about the C_3 axis, although it is not clear if reorientations about other anion symmetry axes, such as the C_2 , are possible. Indeed, except for the poor agreement with the 5-fold rotation about the C_5 symmetry axis, in which two of the 12 H atoms are immobile, there could very well be other possible lower-symmetry axes involving the motions of all 12 H atoms. One must remember that the composite EISF is a sum of the individual EISFs from each $\text{B}_{12}\text{H}_{12}^{2-}$ anion, so there may

be a distribution of axes that yield the observed EISF. Indeed, the fact that the observed EISF values for $0.1 \text{ \AA}^{-1} < Q < 1.4 \text{ \AA}^{-1}$ in the fully disordered phase dip slightly below the values expected for uniaxial reorientation suggests that a minor fraction of the anions have near-neighbor Na^+ cation configurations that lead to multiaxis reorientations (3-D tumbling) instead of uniaxial reorientations. This is exemplified in Figure 7, where the observed EISF values are compared to a

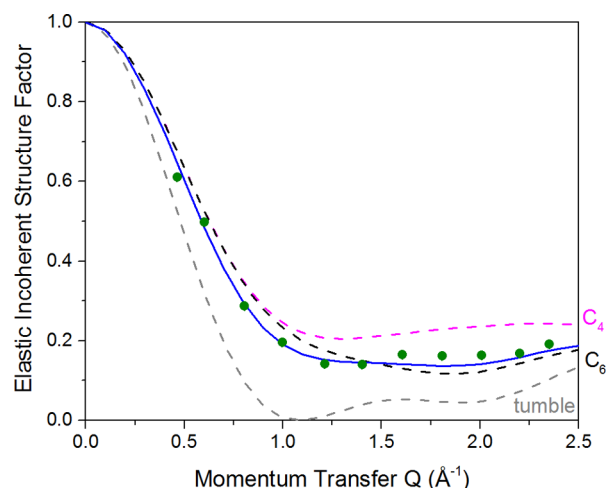


Figure 7. High-temperature QENS data (580 K, green circles) compared with a composite EISF model (blue line) comprised of 50% of the anions undergoing 6-fold jumps around the C_3 axis (black dashes), 30% undergoing 4-fold jumps around the C_2 axis (pink dashes), and 20% undergoing 3-D tumbling (gray dashes).

composite model EISF curve comprised of half of the anions undergoing 6-fold jumps around the C_3 axis, 30% undergoing 4-fold jumps around the C_2 axis and the remaining 20% undergoing 3-D tumbling. Although not a unique model, it illustrates the point that, despite a variety of possible reorientational mechanisms as a result of the disordered Na^+ cation sublattice, anion reorientations tend to be predominantly uniaxial in nature.

Effect of Local Structure on Reorientational Mechanism. Looking at the disordered cubic structure determined by diffraction, one might expect to find an anion reorientational mechanism more akin to 3-D tumbling rather than the observed uniaxial reorientational jump mechanism. To make sense of this mechanism, we must consider both the local structure and the relative mobilities of the cations and anions. Each anion in the fully disordered structure is surrounded by 24 near-neighbor Na^+ cation sites, and each of these cation sites is, on average, one-third occupied.¹⁸ Moreover, as these cation sites are relatively large and distorted tetrahedral interstices, the small cation can occupy various off-center positions. Hence, for any given snapshot in time, each anion will possess one of a variety of near-neighbor cation configurations. Chances are that the configuration will be noncubic and lead to a favored axis for reorientation. Since the Na^+ cation jump rates were found to be at least 2 orders of magnitude less than the anion reorientational jump rates,¹⁹ each anion will undergo many reorientational jumps around this favored axis before it experiences any changes in the local cation configuration. Once the Na^+ cation configuration finally leads to a different favored axis for reorientation, the anion will begin again to undergo reorientations about this new axis.

Up to this point, we have not addressed the mechanistic differences observed in Figure 3 between the $Pm\bar{3}n$ and $Im\bar{3}m$ structures. Since the partially disordered $Pm\bar{3}n$ structure is closely related to the fully disordered $Im\bar{3}m$ structure, and the transition between the two is of a second-order nature, we do not expect significant differences in the reorientational activation energies or the temperature dependences of the lattice constants or jump rates. Both structures possess tetrahedrally coordinated cation interstices surrounding each anion. Even though there are twice as many cation sites for the $Im\bar{3}m$ structure compared to the $Pm\bar{3}n$ structure resulting in more possible near-neighbor Na^+ cation configurations around a given anion, the bonding interactions between anions and cations are similar, as is the propensity for uniaxial reorientation. The main difference is that the less orientationally disordered nature of the anions in the $Pm\bar{3}n$ structure apparently leads to a different preferred reorientation axis and/or jump distance (i.e., 4-fold jumps around the C_2 axis instead of smaller jumps around the C_2 or C_3 axes that are more in agreement with the higher-temperature data). Although we acknowledge that there may be subtle dynamical differences between structure types, the Arrhenius plot in Figure 6 suggests that there is little change in the local physical interactions affecting the anion reorientational dynamics due to the second-order phase transition.

Anion Reorientational Mobility and Cation Superionicity. As mentioned previously,¹⁶ it is desirable to understand the relationship, if any, between the onset of Na^+ superionicity and the dramatic enhancement in $B_{12}H_{12}^{2-}$ anion reorientational mobility. The entropy-driven transformation to the disordered bcc phase from the ordered monoclinic phase leads to a sublattice of Na^+ cation sites reminiscent of the Ag^+ cation sublattice in the bcc α -AgI fast-ion conductor²⁶ and the sublattice of tetrahedral sites in bcc metals that enable fast diffusion of absorbed H atoms.²⁷ This particular sublattice geometry is known to enable more facile jump diffusion (most recently for Li^+ cation diffusion in $LiLa(BH_4)_3Cl^{28}$).

Given the above comparisons, is the role of the $B_{12}H_{12}^{2-}$ anions merely to provide the entropic mechanism to attain the beneficial sublattice geometry, or is the presence of rapid reorientational motions of the anions leading to a further improvement in cation diffusion rates? In the present case, the much higher anion reorientation rates may enhance the cation jump rates by providing multiple opportunities for the cations to move past the rotating anion in a cooperative fashion. Hypothetically, one could test this by slowing down the anion reorientational motion and observing the perturbation, if any, on the Na^+ cation jump rate. The data in Figure 6 suggest that this could be done by comparing the Na^+ jump rates and/or conductivity for $Na_2B_{12}H_{12}$ and $Na_2B_{12}D_{12}$, since the hydrogenated and deuterated anions possess roughly 3-fold different reorientational jump rates. In order to avoid confusion due to lattice constant differences between $Na_2^{11}B_{12}H_{12}$ and $Na_2^{11}B_{12}D_{12}$ ¹⁸ that might affect reorientation rates, one might alternatively try to compare $Na_2^{10}B_{12}H_{12}$ and $Na_2^{11}B_{12}H_{12}$, which are expected to have closer lattice constants, but still possess different moments of inertia. In any case, it remains to be seen whether or not the magnitudes of the rates are too high to measure an observable effect on Na^+ cation mobility. Having said this, we stress that QENS measurements on DCS are only sensitive to reorientational jump rates larger than 10^9 to 10^{10} jumps s^{-1} . Any contributions due to slower jump rates around different axes will be buried within the neutron elastic peak.

Although not probed by QENS, these less frequent jumps may still be significant facilitators for Na^+ translational diffusion.

CONCLUDING REMARKS

Quasielastic neutron scattering (QENS) measurements of the superionic conducting phase of $Na_2B_{12}H_{12}$ were performed to characterize the anion reorientational dynamics. The data suggest that the reorientationally disordered $B_{12}H_{12}^{2-}$ anions undergo rapid reorientational jumps (on the order of 10^{11} jumps s^{-1} at 530 K), predominantly about a single axis, despite the diffraction-average local cubic symmetry, with an activation energy of $259 \text{ meV} \pm 22 \text{ meV}$ ($25 \text{ kJ mol}^{-1} \pm 2 \text{ kJ mol}^{-1}$). Our results are consistent with recent NMR measurements. This is at least 2 orders of magnitude faster than the Na^+ cation diffusional jump rate. This rapid reorientational mobility may very well enhance cation mobility among the tetrahedral interstices of the bcc lattice. More experiments are necessary to determine the nature of the relationship between anion reorientational mobility and cation superionicity.

Besides characterizing the dynamics within bcc sublattice geometries, we are currently exploring the Na^+ cation and $B_{12}H_{12}^{2-}$ anion dynamics within different sublattice geometries, such as the one present in the disordered, face-centered-cubic (fcc) mixed-cation phases of $Li_yNa_{2-y}B_{12}H_{12}$, which we have found to possess $Li_2B_{12}H_{12}$ -like structural behavior^{18,29} with order-disorder transition temperatures intermediate between those of $Li_2B_{12}H_{12}$ and $Na_2B_{12}H_{12}$. The disordered fcc phases of these mixed-cation compounds are also more stable than that of pure $Li_2B_{12}H_{12}$ and more amenable to dynamical measurements. Details will be the subject of a separate publication.

ASSOCIATED CONTENT

Supporting Information

The Supporting Information contains the equations for the rotational models presented in the manuscript. This material is available free of charge via the Internet at <http://pubs.acs.org>.

AUTHOR INFORMATION

Notes

The authors declare no competing financial interest.

ACKNOWLEDGMENTS

This work was partially supported by the DOE EERE through Grant Nos. DE-EE0002978, DE-AI-01-05EE11104, and DE-AC04-94AL85000 and by the Russian Foundation for Basic Research under Grant No. 12-03-00078, the U.S. Civilian Research & Development Foundation (CRDF Global) under Award No. RUP1-7076-EK-12 and the National Science Foundation under Cooperative Agreement No. OISE-9531011. This work utilized facilities supported in part by the National Science Foundation under Agreement DMR-0944772.

REFERENCES

- (1) He, L.; Li, H.-W.; Hwang, S.-J.; Akiba, E. Facile Solvent-Free Synthesis of Anhydrous Alkali Metal Dodecaborate $M_2B_{12}H_{12}$ ($M = Li, Na, K$). *J. Phys. Chem. C* **2014**, *118*, 6084–6089.
- (2) Remhof, A.; Yan, Y.; Rentsch, D.; Borgschulte, A.; Jensen, C. M.; Züttel, A. Solvent-Free Synthesis and Stability of $MgB_{12}H_{12}$. *J. Mater. Chem. A* **2014**, *2*, 7244–7249.
- (3) Soloveichik, G. L.; Gao, Y.; Rijssenbeek, J.; Andrus, M.; Kniajanski, S.; Bowman, R. C.; Hwang, S.-J.; Zhao, J.-C. Magnesium Borohydride as a Hydrogen Storage Material: Properties and

Dehydrogenation Pathway of Unsolvated $\text{Mg}(\text{BH}_4)_2$. *Int. J. Hydrogen Energy* **2009**, *34*, 916–928.

(4) Orimo, S.; Nakamori, Y.; Ohba, N.; Miwa, K.; Aoki, M.; Towata, S.-I.; Züttel, A. Experimental Studies on Intermediate Compound of LiBH_4 . *Appl. Phys. Lett.* **2006**, *89*, 021920.

(5) Hwang, S.-J.; Bowman, R. C.; Reiter, J. W.; Rijssenbeek, J.; Soloveichik, G. L.; Zhao, J.-C.; Kabbour, H.; Ahn, C. C. NMR Confirmation for Formation of $[\text{B}_{12}\text{H}_{12}]^{2-}$ Complexes during Hydrogen Desorption from Metal Borohydrides. *J. Phys. Chem. C* **2008**, *112*, 3164–3169.

(6) Pitt, M. P.; Paskevicius, M.; Brown, D. H.; Sheppard, D. A.; Buckley, C. E. Thermal Stability of $\text{Li}_2\text{B}_{12}\text{H}_{12}$ and Its Role in the Decomposition of LiBH_4 . *J. Am. Chem. Soc.* **2013**, *135*, 6930–6941.

(7) Yan, Y.; Li, H.-W.; Maekawa, H.; Miwa, K.; Towata, S.; Orimo, S. Formation of Intermediate Compound $\text{Li}_2\text{B}_{12}\text{H}_{12}$ during the Dehydrogenation Process of the LiBH_4 – MgH_2 System. *J. Phys. Chem. C* **2011**, *115*, 19419–19423.

(8) Garroni, S.; Milanese, C.; Pottmaier, D.; Mulas, G.; Nolis, P.; Girella, A.; Caputo, R.; Olid, D.; Teixidor, F.; Baricco, M.; et al. Experimental Evidence of $\text{Na}_2[\text{B}_{12}\text{H}_{12}]$ and Na Formation in the Desorption Pathway of the $2\text{NaBH}_4 + \text{MgH}_2$ System. *J. Phys. Chem. C* **2011**, *115*, 16664–16671.

(9) Minella, C. B.; Garroni, S.; Olid, D.; Teixidor, F.; Pistidda, C.; Lindemann, I.; Gutfleisch, O.; Baró, M. D.; Bormann, R.; Klassen, T.; Dornheim, M. Experimental Evidence of $\text{Ca}[\text{B}_{12}\text{H}_{12}]$ Formation During Decomposition of a $\text{Ca}(\text{BH}_4)_2 + \text{MgH}_2$ Based Reactive Hydride Composite. *J. Phys. Chem. C* **2011**, *115*, 18010–18014.

(10) Newhouse, R. J.; Stavila, V.; Hwang, S.-J.; Klebanoff, L. E.; Zhang, J. Z. Reversibility and Improved Hydrogen Release of Magnesium Borohydride. *J. Phys. Chem. C* **2010**, *114*, 5224–5232.

(11) Hwang, S.-J.; Bowman, R. C., Jr.; Kim, C.; Zan, J. A.; Reiter, J. W. Solid State NMR Characterization of Complex Metal Hydrides Systems for Hydrogen Storage Applications. *J. Anal. Sci. Technol.* **2011**, *2*, A159–A162.

(12) Li, H.-W.; Miwa, K.; Ohba, N.; Fujita, T.; Sato, T.; Yan, Y.; Toawata, S.; Chen, M. W.; Orimo, S. Formation of an Intermediate Compound with a $\text{B}_{12}\text{H}_{12}$ cluster: Experimental and Theoretical Studies on Magnesium Borohydride $\text{Mg}(\text{BH}_4)_2$. *Nanotechnology* **2009**, *20*, 204013.

(13) Friedrichs, O.; Remhof, A.; Hwang, S.-J.; Züttel, A. Role of $\text{Li}_2\text{B}_{12}\text{H}_{12}$ for the Formation and Decomposition of LiBH_4 . *Chem. Mater.* **2010**, *22*, 3265–3268.

(14) Lipscomb, W. N. *Boron Hydrides*; W. A. Benjamin, Inc.: New York, 1963.

(15) Longuet-Higgins, H. C.; Roberts, M. d. V. The Electronic Structure of an Icosahedron of Boron Atoms. *P. R. Soc. London A: Mater.* **1955**, *230*, 110–119.

(16) Udovic, T. J.; Matsuo, M.; Unemoto, A.; Verdál, N.; Stavila, V.; Skripov, A. V.; Rush, J. J.; Takamura, H.; Orimo, S. Sodium Superionic Conduction in $\text{Na}_2\text{B}_{12}\text{H}_{12}$. *Chem. Commun.* **2014**, *50*, 3750–3752.

(17) Her, J.-H.; Zhou, W.; Stavila, V.; Brown, C. M.; Udovic, T. J. Role of Cation Size on the Structural Behavior of the Alkali-Metal Dodecahydro-closo-Dodecaborates. *J. Phys. Chem. C* **2009**, *113*, 11187–11189.

(18) Verdál, N.; Her, J.-H.; Stavila, V.; Soloninin, A. V.; Babanova, O. A.; Skripov, A. V.; Udovic, T. J.; Rush, J. J. High-Temperature Phase Transitions in $\text{Li}_2\text{B}_{12}\text{H}_{12}$ and $\text{Na}_2\text{B}_{12}\text{H}_{12}$. *J. Sol. State Chem.* **2014**, *212*, 81–91.

(19) Skripov, A. V.; Babanova, O. A.; Soloninin, A. V.; Stavila, V.; Verdál, N.; Udovic, T. J.; Rush, J. J. Nuclear Magnetic Resonance Study of Atomic Motion in $\text{A}_2\text{B}_{12}\text{H}_{12}$ (A = Na, K, Rb, Cs): Anion Reorientations and Na^+ Mobility. *J. Phys. Chem. C* **2013**, *117*, 25961–25968.

(20) The mention of all commercial suppliers in this paper is for clarity. This does not imply the recommendation or endorsement of these suppliers by NIST.

(21) Copley, J. R. D.; Cook, J. C. The Disk Chopper Spectrometer at NIST: A New Instrument for Quasielastic Neutron Scattering Studies. *Chem. Phys.* **2003**, *292*, 477–485.

(22) Azuah, R. T.; Kneller, L. R.; Qiu, Y.; Tregenna-Piggott, P. L. W.; Brown, C. M.; Copley, J. R. D.; Dimeo, R. M. DAVE: A Comprehensive Software Suite for the Reduction, Visualization, and Analysis of Low Energy Neutron Spectroscopic Data. *J. Res. Natl. Inst. Stand. Technol.* **2009**, *114*, 341–358.

(23) Verdál, N.; Udovic, T. J.; Rush, J. J.; Cappelletti, R. L.; Zhou, W. Reorientational Dynamics of the Dodecahydro-closo-dodecaborate Anion in $\text{Cs}_2\text{B}_{12}\text{H}_{12}$. *J. Phys. Chem. A* **2011**, *115*, 2933–2938.

(24) Bée, M. *Quasielastic Neutron Scattering, Principles and Applications in Solid State Chemistry, Biology and Materials Science*; Adam Hilger: Bristol, U.K., 1988.

(25) Dianoux, A. J.; Volino, F.; Hervet, H. Incoherent Scattering Law for Neutron Quasi-Elastic Scattering in Liquid Crystals. *Mol. Phys.* **1975**, *30*, 1181–1194.

(26) Nield, V. M.; Keen, D. A.; Hayes, W.; McGreevy, R. L. Structure and Fast-Ion Conduction in Alpha-AgI. *Sol. State Ionics* **1993**, *66*, 247–258.

(27) Fukai, Y. *The Metal–Hydrogen System*; Springer: Berlin, 1993.

(28) Skripov, A. V.; Soloninin, A. V.; Ley, M. B.; Jensen, T. R.; Filinchuk, Y. Nuclear Magnetic Resonance Studies of BH_4 Reorientations and Li Diffusion in $\text{LiLa}(\text{BH}_4)_3\text{Cl}$. *J. Phys. Chem. C* **2013**, *117*, 14965–14972.

(29) Paskevicius, M.; Pitt, M. P.; Brown, D. H.; Sheppard, D. A.; Chumphongphan, S.; Buckley, C. E. First-Order Phase Transition in the $\text{Li}_2\text{B}_{12}\text{H}_{12}$ system. *Phys. Chem. Chem. Phys.* **2013**, *15*, 15825–15828.